STATISTICAL CLASSIFICATION OF THE COMPOSITION OF MAFIC-RICH MARTIAN TERRAINS FROM ORBITAL OBSERVATIONS. L. Riu[1], F.Poulet[1], J-P.Bibring[1], B.Gondet[1]. [1]Institut d'Astrophysique Spatiale, Université Paris-Sud, 91405 Orsay cedex, France. Contact: lucie.riu@ias.u-psud.fr

Introduction: The volcanic and magmatic history of Mars can be traced thanks to the knowledge of its surface composition. Previous past orbital and *in situ* analyses have shown that the Martian crust consists of volcanic basalt [e.g. 1] dominated by plagioclase, pyroxenes and olivine [2,3,4]. The compositional associations with terrain age, geologic setting, and surface properties, can be then used to infer processes and events which produced those compositions.

Instead of looking at each mineral spatial distribution separately, we present here a statistical approach to highlight distinct mineralogical assemblages modeled from OMEGA data at a spatial resolution of 32 px/° in order to associate the surface composition to magmatic mechanisms and potentially show an evolution with time.

Dataset: The study presented here is based on modal mineralogy inferred from OMEGA near-infrared reflectance spectra. This global product was derived by several steps. All available observations for global mineralogical studies were first combined into a 3-D global reflectance cube of the Martian surface from a processing pipeline detailed in [5]. Then, a radiative transfer model based on the Shkuratov theory [6] was applied to each spectrum of this global cube that exhibits pyroxene signature in order to derive abundances and grain sizes of 5 end-members at the global scale. The granular mixture able to reproduce the spectral properties of mafic terrains is composed of two poles of pyroxenes (low- and high- calcium pyroxene, respectively LCP and HCP), plagioclase (labradorite), olivine (Mg-rich forsterite) and a dust analog ([7,8]). These global abundance maps show mineralogical distributions of the minerals previously mentioned at km scale (~1.5 km/px) from 60°S to 30°N in latitude [9]. This results in about 8 millions pixels. The last step consists in applying a standard statistical method to these global maps of mineral abundances. For each end-member, its abundance was normalized prior to conduct the classification by substracting the average abundance and dividing by the standard deviation for each pixel. This additional processing step is carried out to prevent bias on the resulting classification map based on the dispersion of abundances for each of the five parameters.

Classification method: We use *k-means* clustering to highlight distinct mineralogical assemblages. This statistical approach aims at partitioning the pixels in order to maximize the distance between each parameter (i.e abundance) of the distinct clusters. For the *k-means* clustering method, the number of classes needs to be initialized. Based on previous, TES [10] and OMEGA [9] statistical analyses, we explored several possibilities between 2 to 15 clusters. A method to estimate the appropriate number of clusters is to look at the percentage of explained variance of the dataset with respect to the number of clusters. We show that this parameter stabilizes for 7 clusters, hence the number of clusters was initialized to this value.

Results: Figure 1 illustrates the spatial distribution of all classes and their corresponding averaged abundance values and standard deviations as well as the percentage associated to each class. Their proportion associated to the three major geological eras is shown

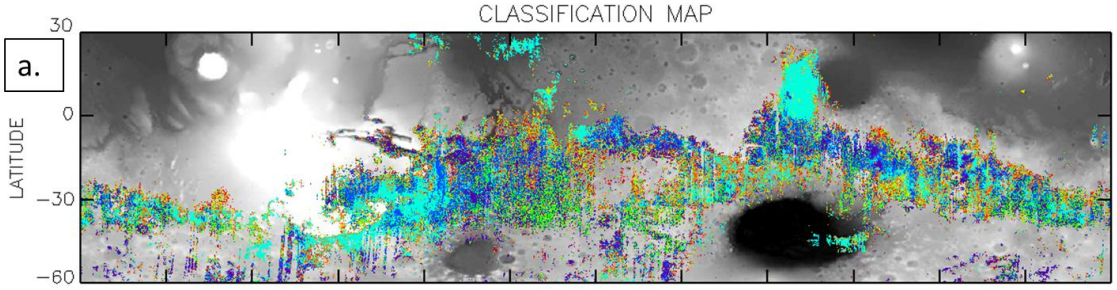

	Class 1	Class 2	Class 3	Class 4	Class 5	Class 6	Class 7
% pixels	13	21	22	11	10	18	5
Dust	3.8 ± 2.3	3.3 ± 1.5	3.6 ± 1.5	2.9 ± 1.7	3.8 ± 1.9	8.1 ± 2.0	13.9 ± 3.2
HCP	22.6 ± 3.3	22.3 ± 2.6	25.0 ± 2.8	23.1 ± 3.5	33.0 ± 4.2	25.0 ± 2.6	26.2 ± 4.0
LCP	15.7 ± 2.8	13.8 ± 2.4	11.9 ± 2.5	24.9 ± 4.5	13.6 ± 3.5	15.2 ± 2.4	18.0 ± 3.0
Olivine	11.7 ± 3.0	6.6 ± 2.0	1.1 ± 1.4	3.6 ± 2.9	3.5 ± 3.1	1.9 ± 2.1	2.4 ± 2.9
Plagioclase	45.0 ± 3.7	52.2 ± 2.9	56.4 ± 3.2	43.6 ± 4.2	45.0 ± 4.6	48.9 ± 3.0	38.9 ± 5.4
% of pixels N/H/A	88.8/11/0.2	87/12.98/0.02	76.99/23/0.01	90/9.97/0.03	82.7/17/0.3	89.98/10/0.02	87.01/13.02/0.07

Figure 1 – (a) Classification map. The color corresponding to each class are shown on Table 1. (b) Average abundances (in wt%) of each class and standard deviation (±Δ). The percentage of pixels per geological era is also indicated. For each class, the abundance in red represents the end-member that strongly dominates the class and conversely the abundance written in blue corresponds to the end-member(s) that is minor.

on Figure 2. For each class, we also compare the results to the GRS chemical abundance maps [11,12]. To do so, the spatial resolution of the OMEGA classification map is degraded to the GRS spatial resolution of 5 × 5° per pixel and we use a mask on the GRS maps to provide the same spatial distribution as the one provided by the OMEGA global abundance maps.

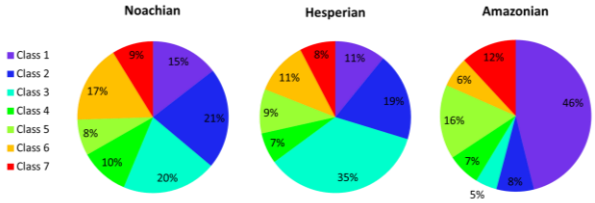

Figure 2 - Pie chart representing the percentage of pixels associated to each class for the three geological eras. The number of pixels per era is normalized.

The classes significantly differ in terms of modal mineralogy and are spatially distinct (Figure 1a). The first class (purple on Fig. 1a) is characterized by the largest olivine abundance (the average abundance being 4.5 wt%). This class is mostly found in Valles Marineris and correspond to half of the pixels associated to the Amazonian era (Figure 2). However, we sample less than 1% of Amazionan aged terrains, so that it is difficult to conclude whether those olivine enriched terrains are representative of this era. When comparing to GRS data, we find that this class appears depleted in Si and Fe compared to the average GRS values (Figure 3), which is consistent with a more mafic composition. This result also reinforces the use of Mg-rich olivine compared to Fe-rich olivine in these regions. Class 2 is an "average" cluster with abundances close to the global averaged abundances obtained on the overall surface [9]. This class corresponds to pixels close to the equator and in the mid-southern latitudes. Class 3 differs from the rest with a higher percentage of Hesperian aged terrains (23 %) which corresponds to more than a third of the overall Hesperian modelled terrains (Fig. 2). This class is found in Syrtis Major, Acidalia Planitia and close to Thaumasia Planum in Protei Regio and Bosporos Planum. It is strongly enriched in plagioclase with an average abundance close to 60 wt%. This class is the only one that shows depletion in incompatible elements K and Th (Figure 3). This observation suggests that those terrains were formed through high degree of partial melting [13], but this is in contradiction with the high percentage of plagioclase that corresponds to low degree of partial melting. However, the content of incompatible elements strongly depends on previous melting [13] and may thus not be the best tracer to account for high degree of partial melting compared to LCP. The Class 4 is characterized with an enrichment in LCP. This class do not account for a large percentage of pixels (11 %) and is spatially restricted to Noachis Terra. This observation is in good agreement with the previous local [2,14] and global [9,10] observations that showed that LCP is associated with older terrains and that its content is decreasing with time with regards to the total pyroxene content.

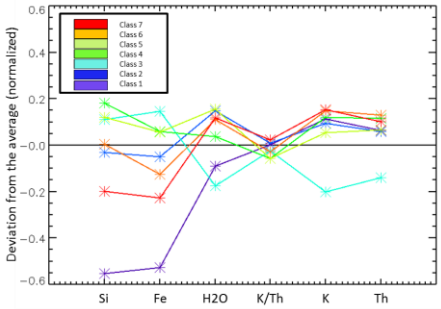

Figure 3 - Normalized GRS abundances distribution for each OMEGA class compared to the average value on all pixels. Each abundance is normalized to be plotted on the same graph.

Conclusion: The statistical approach presented here shows that 7 distinct mineralogical assemblages could be highlighted based on the global OMEGA-based abundance maps [9]. The clusters differ through their assemblages with various major mineral : olivine, LCP, HCP or plagioclase and thus show real differences in terms of mineralogy. Nevertheless, except for class 3 that regroups a majority of Hesperian aged terrains, this global and kilometric approach does not highlight an evolution in terms of composition with time and mainly suggests a certain spatial heterogeinity through time for both Noachian and Hesperian terrains. However, previous investigations have demonstrated the importance to carefully look for any correlation between mineral variability and local geological settings [15]. Local and regional analyses are thus foreseen to see whether additional various and complexe magmatic episodes could be inferred.

References: [1] McSween et al., (2009), *Science*, 324. [2] Poulet et al., (2009), *Icarus*, 201. [3] Bandfield, (2002), *JGR*, 107. [4] Rogers and Christensen, (2007), *JGR*, 112, E01003. [5] Riu et al. (2018), *submitted*. [6] Shkuratov et al. (1999), *Icarus, 137*. [7] Poulet et al. (2007), *JGR, 112*, E08S02. [8] Ody et al. (2012), *JGR, 117*, E00J14. [9] Riu et al. (2017), *LPSC 48*, Abstract #1815. [10] Rogers & Hamilton (2015) *JGR, 120*, 62–91. [11] Boynton et al. (2007), *JGR, 112*, E12S99. [12] Taylor et al. (2006), *JGR, 111*, E03S10. [13] Baratoux et al. (2011) *Nature, 472, 338-341*. [14] Mustard et al. (2005), *Science, 307*. [15] Ody et al. (2013), *JGR*, 243-262.